JCTC Journal of Chemical Theory and Computation

Article

pubs.acs.org/JCTC

Curvature Effect on the Capacitance of Electric Double Layers at Ionic Liquid/Onion-Like Carbon Interfaces

Guang Feng,[†] De-en Jiang,[‡] and Peter T. Cummings*[,†,§]

[†]Department of Chemical and Biomolecular Engineering, Vanderbilt University, Nashville, Tennessee 37235, United States

[‡]Chemical Sciences Division and [§]Center for Nanophase Materials Sciences, Oak Ridge National Laboratory, Oak Ridge, Tennessee 37831, United States

Supporting Information

ABSTRACT: Recent experiments have revealed that onion-like carbons (OLCs) offer high energy density and charging/discharging rates when used as the electrodes in supercapacitors. To understand the physical origin of this phenomenon, molecular dynamics simulations were performed for a room-temperature ionic liquid near idealized spherical OLCs with radii ranging from 0.356 to 1.223 nm. We find that the surface charge density increases almost linearly with the potential applied on electric double layers (EDLs) near OLCs. This leads to a nearly flat shape of the differential capacitance versus the potential, unlike the bell or camel shape observed on planar electrodes. Moreover, our simulations reveal that the capacitance of EDLs on OLCs increases with the curvature or as the OLC size decreases, in agreement with experimental observations. The curvature effect is explained by dominance of charge overscreening over a wide potential range and increased ion density per unit area of electrode surface as the OLC becomes smaller.

1. INTRODUCTION

As a novel class of energy storage devices, electrical double layer (EDL) capacitors, also called supercapacitors or ultracapacitors, have attracted considerable attention, owing to their advantageous properties, such as high power density, high capacitance, and excellent durability.[1,2] With high specific surface area (SSA) and electrical conductivity,[2−4] carbon-based materials are the most widely used electrodes for supercapacitors, including activated carbons, templated and carbide-derived carbons (CDC),[4,5] carbon fabrics,[4] carbon fibers,[6] carbon nanotubes (CNTs),[7] and graphene-based composites,[8] among others. For instance, Korenblit et al.[9] produced ordered mesoporous CDC materials to enhance the SSA of electrodes as well as the capacitance of supercapacitor, by selective etching of metal carbides in a chlorine-containing environment. Single-wall CNTs were assembled into ultrathin long fibrils to improve both conductivity and capacitive performance of carbon electrodes in supercapacitors, through a dielectrophoretic technique.[10]

Recently, onion-like carbons (OLCs) have emerged as a novel type of electrode materials for supercapacitors.[11−14] Formed by vacuum annealing of nanodiamond powder, OLCs can be viewed as concentric graphene shells, and their surface is fully accessible for ion accumulation.[13,15,16] Using voltammetric technique, Bushueva et al.[13] reported that supercapacitors based on OLCs in KOH alkaline solution exhibit a specific capacitance comparable with those of other modern carbon materials.[8,17,18] Moreover, EDL capacitors with OLCs in H_2SO_4 acidic solution exhibit favorably rapid response, as obtained by the cavity microelectrode technique.[11] Using OLC-based electrodes with a nonaqueous electrolyte of tetraethylammonium tetrafluoroborate in propylene carbonate, Pech et al.[12] found that such supercapacitors have not only high energy density but also ultrahigh power density due to the OLC surface accessibility. Furthermore, it has been shown by Huang et al.[19] that the EDL capacitance increases as the OLC becomes smaller, but the origin of such curvature effects is still unclear.

In addition to aqueous and organic electrolytes, room-temperature ionic liquids (RTILs) have become promising candidates for electrolytes used in supercapacitors, because of their wide electrochemical windows, excellent thermal stability, nonvolatility, relatively inert nature, and good ionic conductivity.[17,20,21] The EDLs at the interfaces of RTILs and planar electrodes have been studied extensively. Ions, especially cations with the imidazolium ring, are found to adsorb on neutral planar electrodes.[22−24] Several research groups observed that the cations and anions form alternating layers near the charged electrodes due to the strong cation−anion correlations and the layering penetrates about 1.0−2.5 nm (depending on the ion size and applied potentials) into the RTIL bulk.[23−28] Theory and simulations demonstrated that charge overscreening is a universal feature of EDLs due to the high ionic density and strong ion coupling in RTILs.[24,29−31]

Besides EDL structures at the RTIL/planar electrode interfaces, the differential capacitance versus the electrode potential ($C−V$) has been investigated extensively in theory, simulation, and experiment. Analytical theories showed a transition of the $C−V$ curve from the camel to the bell shape with the ionic density.[29,32] This transition was confirmed by modified Poisson−Boltzmann theory[33] and classical density functional theory.[27] Both Monte Carlo and molecular dynamics (MD) simulations have been used to explore the $C−V$ curve of the RTIL on the planar electrode where either a bell or a camel shape was obtained.[26,34,35] Experimentally, the U, bell, and

Received: December 20, 2011
Published: February 2, 2012

camel shapes of the $C-V$ curves were all observed at the RTIL/planar electrode interfaces.[36−39]

Despite the tremendous amount of theoretical and modeling work on the capacitance of RTILs at the planar electrode and two recent MD studies of RTILs inside and outside CNT electrodes,[24,40] very little is known about how the EDLs in RTILs would be affected by the spherical shape of electrodes like OLCs. Given the recent discovery[12] of ultrahigh power density from OLC-based supercapacitors, it would be desirable to understand: How would the EDL structure and capacitance change as the OLC becomes smaller? and would the shape of the $C-V$ curve be different on OLCs from on the planar electrode? In this work, we employ atomistic MD simulations to answer these important questions regarding the EDLs at the interfaces of RTILs near OLCs.

2. COMPUTATIONAL METHODS

As Figure 1 shows, we simulated the structure and dynamics of the RTIL 1-ethyl-3-methylimidazolium bis-(trifluoromethylsulfonyl)imide ([emim][Tf_2N]) in contact exohedrally with neutral and charged OLCs of various radii (R = 0.356, 0.610, 0.705, 0.814, 1.018, and 1.223 nm). Herein, our model for an OLC consists of two or three concentric graphitic shells. In each OLC, the gap between two shells is 0.336 nm along the radial direction.[2] Small partial charges were placed on a spherical image surface that is 0.07 nm away from the outside shell of each OLC to produce a potential drop across each EDL.[41] The simulation box size was chosen to be $2(R + 3)$ nm in all three dimensions so that the electrolyte far from the electrode adopts bulk-like behavior and the EDL does not overlap with its image (thus the electrical potential profile is flat there). The force fields for the electrode atoms (carbon) and ions were taken from ref 42.

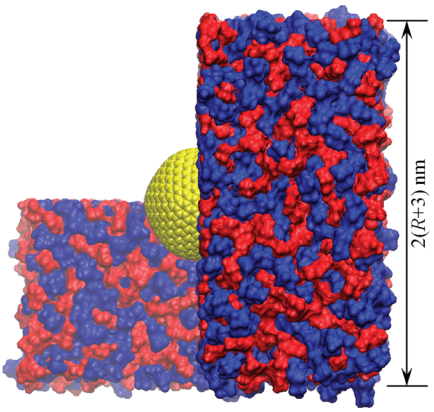

Figure 1. Snapshot of the MD simulation system. Section planes are used to show the modeled OLC (yellow spheres) with a radius of R. The red and blue spheres denote $emim^+$ and Tf_2N^- ions, respectively. Periodic boundary conditions were used in all three dimensions.

Simulations were performed in the NPT ensemble using a customized MD code based on the Gromacs 3.3 software.[43] The IL temperature was maintained by using the Berendsen thermostat with a time constant of 1.0 ps. The electrostatic interactions were computed using the PME method.[44] Specifically, an FFT grid spacing of 0.10 nm and cubic interpolation for charge distribution were used to compute the electrostatic interactions in reciprocal space. A cutoff distance of 1.1 nm was used in the calculation of electrostatic interactions in the real space. The nonelectrostatic interactions were computed by direct summation with a cutoff length of 1.1 nm. The LINCS algorithm[45] was used to maintain the bond lengths within the $emim^+$ cation and Tf_2N^- anion. Each simulation was started at 1000 K and subsequently annealed gradually to 298 K in 6 ns. Following annealing, the system was maintained at 298 K for another 6 ns to reach equilibrium. Finally, a 9 ns production run was performed. To ensure the statistical accuracy of the simulation results, an ensemble of three MD trajectories with independent initial configurations was utilized.

In this work, to compute the capacitance of the EDL adjacent to each OLC, the method described in ref 24 for the planar electrode (in which structural and charge data was accumulated in bins parallel to the surface) was adopted, using spherical-shell bins instead. Briefly, the electrical potential distribution along the radial direction of electrodes was computed by solving the Poisson's equation using the space charge density obtained in MD simulations as input. Then, the electrical potential drop across each EDL, ϕ_{EDL}, was determined from the electrical potential distribution, $\phi(r)$, which can be calculated by

$$\phi(r) = -\frac{1}{\varepsilon_0}\int_R^r \left(1 - \frac{u}{r}\right) u\rho_e(u)\,du - \frac{\sigma R}{\varepsilon_0}\left(1 - \frac{R}{r}\right) \quad (1)$$

where $\rho_e(u)$ is the space charge density from the outermost surface of OLCs to the bulk RTILs along the radial direction, R is the radius of an OLC, σ is the surface charge density of the electrode, and ε_0 is the vacuum permittivity. Based on eq 1, as σ = 0, the potential difference between electrode and bulk electrolyte, i.e., potential of zero charge (PZC), was found to be similar in value (−174 ± 19 mV) for different OLCs (See Figure S1 in Supporting Information for the charge density and corresponding potential distribution across EDLs near neutral electrodes). Since PZC is not zero for all simulation systems, $V_{EDL} = \phi_{EDL} - PZC$ was considered as the potential applied on each EDL for convenience.

Additionally, simulations were performed to study the structure and capacitance of EDLs near planar electrodes, separated widely enough to create a region of bulk fluid between the two electrodes, which could provide a baseline for curved electrodes. Similar to those in ref 46, the IL was enclosed between two oppositely charged channel walls which were modeled by three layers of graphene sheets.

3. RESULTS AND DISCUSSION

For an OLC of a specific radius, we examined the EDLs of the RTIL [emim][Tf_2N] at various surface charge densities (σ) and obtained the potential applied on EDLs ($V_{EDL} = \phi_{EDL} - PZC$, see the Computational Methods Section). We found that for each OLC, the surface charge density almost increases linearly with the applied potential, quite unlike that on the planar electrode. This contrast of behavior is more easily visualized if we look at the differential capacitance computed as $C = d\sigma/dV_{EDL}$. Figure 2 shows the capacitance−electrode potential ($C-V$) curves of EDLs near electrodes with different spherical curvatures. Unlike the U, bell, or camel shapes on the planar electrode, we observe a roughly flat $C-V$ curve for the OLC electrodes. This distinct behavior becomes more pronounced as the OLC becomes smaller; for example, the OLC with a radius (R) of 0.705 nm in comparison with that of R = 1.223 nm (Figure 2). This unique behavior of nearly flat $C-V$ curve at

dx.doi.org/10.1021/ct200914j | J. Chem. Theory Comput. 2012, 8, 1058−1063

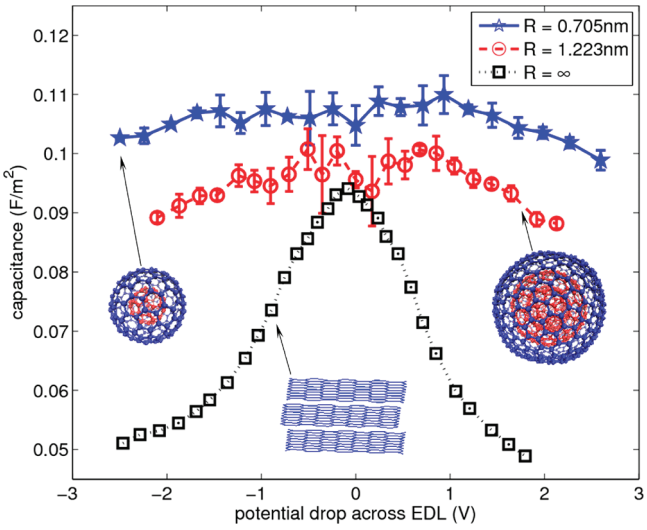

Figure 2. Influence of electrode curvature on differential capacitance. R is the radius of an OLC and is infinity for the planar electrodes.

OLC electrodes will potentially inspire the design of supercapacitors with stable capacitive performance.

To understand the difference of the $C-V$ relationship between OLCs and the planar electrode, we first focus on the planar electrode where the bell-shaped $C-V$ curve seen herein is consistent with previously published work[47] and can be attributed to the charge overscreening at the small/moderate voltages and lattice saturation at large voltages.[48] Figure 3

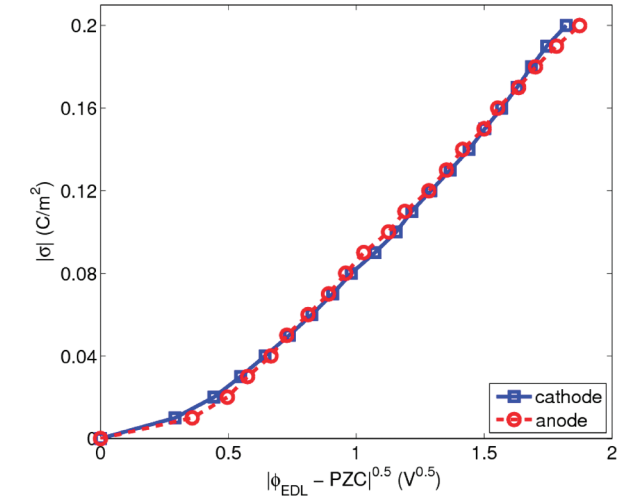

Figure 3. Surface charge density as a function of the square root of electrode potential: lattice saturation occurs at moderate potentials applied on planar electrodes.

shows the relation between the absolute value of surface charge density and the square root of the applied potential ($|V_{EDL}|$) for EDLs near cathode ($emim^+$ ion as the counterion) and anode (Tf_2N^- ion as the counterion). We observe that lattice saturation takes place at a moderate potential (where $|\sigma| \propto |V_{EDL}|^{0.5}$ holds), i.e., the saturation voltage is approximately −1.0 V on the cathode side and 0.8 V on the anode side, in agreement with results from Monte Carlo simulations and experiments.[34,39] Consequently, the wing of $C-V$ curve, beyond the region of $-1.0\ V < V_{EDL} < 0.8\ V$, should decrease as the planar electrode becomes more charged due to lattice saturation. Within this potential range, the charge overscreening dictates the $C-V$ shape.[48] To quantify the overscreening, we introduce a charge screening factor

$$C_f(z) = -\int_0^z \Delta\rho_e(s)\mathrm{d}s/\sigma \tag{2}$$

near planar electrodes, and

$$C_f(r) = -\int_R^r \frac{s^2}{R^2}\Delta\rho_e(s)\mathrm{d}s/\sigma \tag{3}$$

near spherical electrodes, where $\Delta\rho_e$ is the variation of space charge density as the surface charge density changes from 0 to σ. $C_f = 1.0$ indicates that the electrode charge gets exactly balanced, while $C_f > 1.0$ means the charge overscreening occurs. Figure 4 shows the charge screening factors, computed by eq 2,

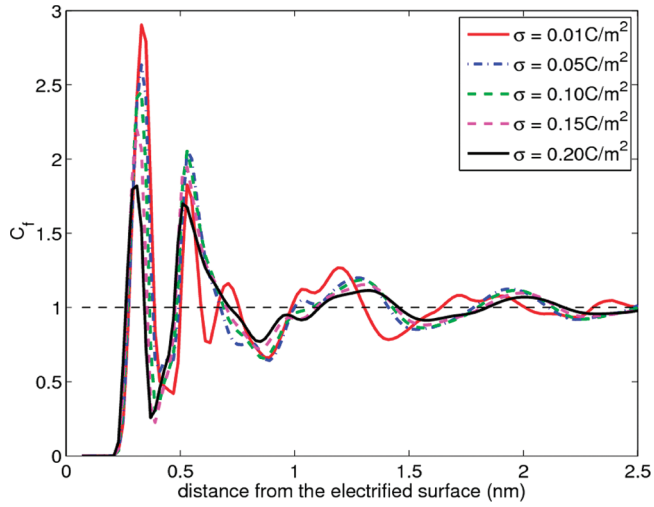

Figure 4. C_f across EDLs in the RTIL [emim][Tf_2N] near positively charged planar electrodes.

near planar electrodes with different positive surface charge densities, where we take the height of the first peak of the charge screening factor as the overscreening factor, β, to quantitatively represent the charge overscreening of an EDL. We observe that the charge overscreening becomes weaker as the electrode becomes more positively charged. The same trend was observed for β of EDLs near negatively charged electrodes. The decreasing overscreening accounts for the decrease of capacitance of EDLs under the potential ranging from zero to the saturation voltage beyond which lattice saturation dominates.[48]

The $C-V$ curve of the EDL near OLC with radius of 0.705 nm is almost independent of the electrode potential applied (the mean of this $C-V$ curve is $0.106 \pm 0.003\ F/m^2$). How can we understand the nearly flat $C-V$ curve from the lattice saturation and charge ovescreening? First, as the spherical curvature of electrode surface increases, the saturation voltage would increase as well, since more curved surface facilitates more ions packing on the electrodes. Our simulations show that, for the electrode with radius of 0.705 nm, the surface charge density is linearly proportional to the electrode potential (Figure S2, Supporting Information) rather than its square root. This indicates that the saturation voltage for an OLC electrode is beyond the potential range of −2.5 to 2.6 V (Figure 2) and much larger than that for planar electrodes. Second, based on eq 3, the charge screening factors near the spherical electrode

with radius of 0.705 nm were plotted in Figure 5. Unlike that for the planar electrode, the overscreening factor (β = 2.38 ± 0.08) changes very little with increasing surface charge density. Hence, the nearly constant charge overscreening dominates in the voltage range of our simulations with OLCs studied, yielding an almost constant differential capacitance of EDLs near the spherical electrodes.

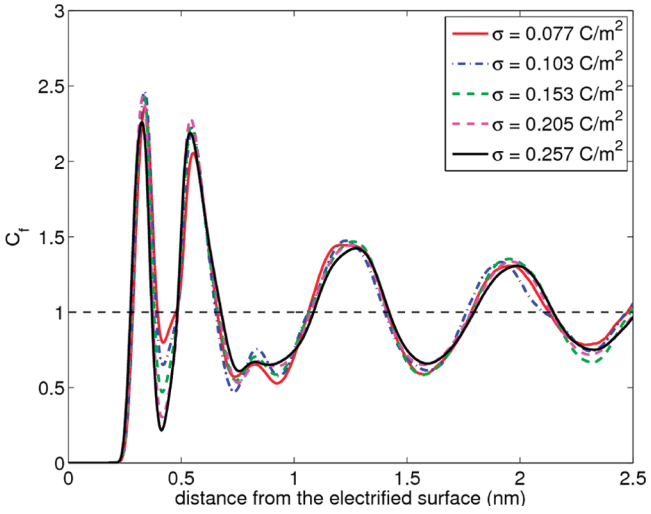

Figure 5. The charge screening factor (C_f) across EDLs in the RTIL [emim][Tf_2N] near spherical electrodes (R = 0.705 nm) with different surface charge densities.

Now we examine how the capacitance at the same applied potential changes with the curvature. The experimental voltage range depends on the electrolyte used; a 2.5−3.0 V range is common for nonaqueous electrolytes. So we chose a voltage range of −1.4 to 1.4 V to compute the integral capacitance by $C = \sigma/V_{EDL}$ for OLCs of different radii (Figure 6), which reveals

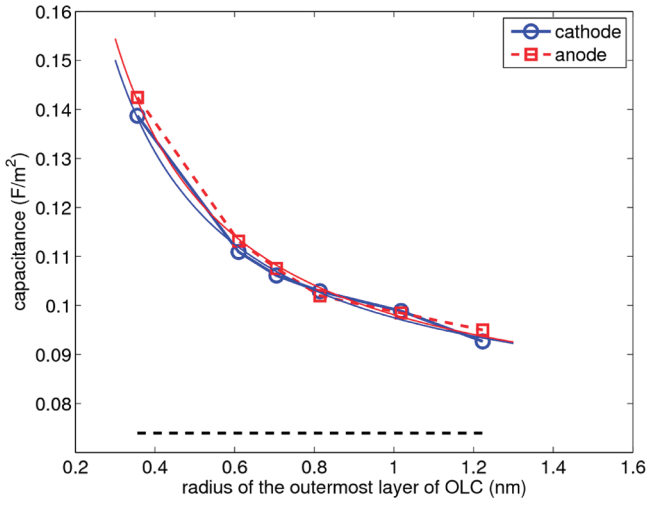

Figure 6. Relation between integral EDL capacitance and the OLC radius. The black dashed line shows the integral capacitance for a planar graphene electrode (the equivalent of radius of infinity).

that the capacitance increases as the OLC become smaller or the curvature increases. We note here that the capacitance is normalized to the surface area of the electrode. We can understand this increase of capacitance with the curvature from the packing of cations and anions near the electrode. As the OLC becomes smaller, more ions can accumulate at the same area of the electrode. Such an accumulative ability of ions can be quantified by counting the ion number in a layer (called layer I) near a unit area of the electrode surface. Layer I was chosen as the region near the cathode or the anode where the charge overscreening dominates. For the Tf_2N^- anion near the positively charged electrode under an applied potential of 1.4 V, this layer extends to about 0.66 nm from the electrode surface; for the $emim^+$ cation near the negatively charged electrode under −1.4 V, it extends to about 0.71 nm. Beyond layer I, both the layering of cation/anion (Figure S3, Supporting Information) and the oscillation of C_f (Figure S4, Supporting Information) become weaker. The thickness of this layer varies only slightly with the OLC radius (Figure S4, Supporting Information). Therefore, the number of counterions within this layer I region is plotted against the OLC radius in Figure 7 for

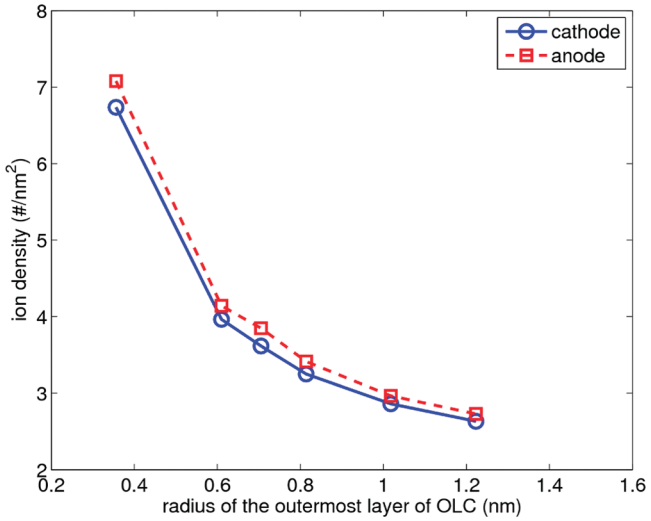

Figure 7. Accumulative ability of counterions near OLCs with different radii.

both the cathode and the anode. One can see that under the same applied potential, more counterions per unit area of the electrode surface are packed in layer I as the OLC becomes smaller. Hence the capacitance normalized to the electrode surface area increases with the curvature, which may explain the larger capacitance of EDLs at ILs/graphite interfaces due to the electrode surface topography characterization.[49]

Essentially, the stronger accumulative ability of counterions on the charged OLCs is attributed to the OLC curvature, which can be better understood by examining the microstructure of EDLs near the neutral electrodes (Figures S5 and S6, Supporting Information). The EDL structures indicate that a larger curvature of the electrode tends to weaken the adsorption of ions, which facilitates more counterions packing on and more co-ions leaving from the electrode surface in the presence of surface charge. Therefore, a larger EDL capacitance can be achieved near a smaller OLC.

The capacitance−radius relation for the exohedral supercapacitor was explored previously,[19] in a phenomenological scaling equation of the form

$$C = \varepsilon_r \varepsilon_0 \left(\frac{1}{R} + \frac{1}{d_{EDL}} \right) \quad (4)$$

dx.doi.org/10.1021/ct200914j | J. Chem. Theory Comput. 2012, 8, 1058−1063

where d_{EDL} is the effective thickness of an EDL and ε_r is the dielectric constant of the EDL near spherical electrode. Fitting simulation results (Figure 6) to eq 4 gives ε_r = 2.54 for EDLs near the cathode and ε_r = 2.73 for the anode, which are both larger than the vacuum value of 1. The values d_{EDL} = 0.30 nm for EDL near the cathode and d_{EDL} = 0.33 nm for EDL near the anode are also reasonable compared with our previous work.[46] The larger dielectric constant of EDL near the anode may result from the more distributed partial charges on the anions, and the larger size of Tf_2N^- ion accounts for the thicker EDL near the anode. As the spherical curvature becomes zero (i.e., planar electrode), eq 4 reduces to $C = \varepsilon_r\varepsilon_0/d_{EDL}$, which is the model for planar capacitors.[19,50] With ε_r and d_{EDL} obtained for the above fitting, one can predict the EDL capacitance near planar electrodes: 0.075 F/m^2 (0.073 F/m^2) for EDL near cathode (anode). These predicted capacitances are very close to the integral capacitance of EDLs near the planar electrode (i.e., ~0.074 F/m^2, Figure 6). Hence our simulation results here are consistent with the phenomenological scaling of capacitance versus radius for the exohedral supercapacitor.[19] The different magnitude of the capacitance compared with experiments may be ascribed to the defects on the OLCs,[12,19,51] since in real systems the defects could make the electrode surface rougher and form some nanopores:[51] The roughness of the electrode surface would change qualitatively the shape of $C-V$ curve, and nanopores on the electrode could change the magnitude of capacitance.[49,50,52−54]

4. CONCLUSIONS

In summary, we studied the effects of electrode curvature on the EDL capacitance of a RTIL electrolyte by atomistic molecular dynamics simulations. An almost linear relationship of the surface charge density versus the electrode potential applied over a large voltage range was found for the EDLs of the IL near the spherical OLC electrodes. This led to a nearly flat curve of the differential capacitance versus the electrode potential ($C-V$), in contrast with the U-, bell-, or the camel-shaped curves observed in many theoretical, simulation, and experimental studies of RTILs on the planar electrode. The flat $C-V$ curve was ascribed to an almost constant charge overscreening which dominates in the simulated voltage range. Since [emim][Tf_2N] is a typical ionic liquid, we hypothesize that this new curvature-induced feature may also hold for other ionic liquids, and additional simulations are currently on the way to test this hypothesis. We also found that the normalized capacitance increases with the OLC size decreasing, in line with experimental results. This increase with the curvature was explained by the enhanced ion density per unit area of the electrode surface as the OLC becomes smaller. To date there have been few experimental studies utilizing OLC-based supercapacitors with ILs. The novel and very promising features of the EDLs in ILs near OLCs, revealed in our simulations reported herein, invite further experimental exploration to take advantage of this phenomenon.

■ ASSOCIATED CONTENT

Supporting Information

Details of surface charge density vs the applied potential on the EDL near OLC and the microstructures of electrical double layers in ionic liquids. This material is available free of charge via the Internet at http://pubs.acs.org.

■ AUTHOR INFORMATION

Corresponding Author

*E-mail: peter.cummings@vanderbilt.edu.

Notes

The authors declare no competing financial interest.

■ ACKNOWLEDGMENTS

This work is supported as part of the Fluid Interface Reactions, Structures, and Transport (FIRST) Center, an Energy Frontier Research Center funded by the U.S. Department of Energy, Office of Science, Office of Basic Energy Sciences, under award number ERKCC61. The authors appreciate the Palmetto cluster at Clemson University and the National Energy Research Scientific Computing Center for providing computer time. G.F. gratefully acknowledges valuable discussions from Dr. Volker Presser at Drexel University.

■ REFERENCES

(1) Conway, B. E. *Electrochemical Supercapacitors: Scientific Fundamentals and Technological Applications*; Kluwer Academic/Plenum Publishers: New York, 1999.

(2) Simon, P.; Gogotsi, Y. *Nat. Mater.* **2008**, *7*, 845−854.

(3) Hu, L.; Pasta, M.; Mantia, F. L.; Cui, L.; Jeong, S.; Deshazer, H. D.; Choi, J. W.; Han, S. M.; Cui, Y. *Nano Lett.* **2010**, *10*, 708−714.

(4) Zhang, L. L.; Zhao, X. S. *Chem. Soc. Rev.* **2009**, *38*, 2520−2531.

(5) Dash, R.; Chmiola, J.; Yushin, G.; Gogotsi, Y.; Laudisio, G.; Singer, J.; Fischer, J.; Kucheyev, S. *Carbon* **2006**, *44*, 2489−2497.

(6) Barranco, V.; Lillo-Rodenas, M. A.; Linares-Solano, A.; Oya, A.; Pico, F.; IbanÃÉez, J.; Agullo-Rueda, F.; Amarilla, J. M.; Rojo, J. M. *J. Phys. Chem. C* **2010**, *114*, 10302−10307.

(7) Asaka, K.; Mukai, K.; Sugino, T.; Kiyohara, K.; Takeuchi, I.; Terasawa, N.; Aida, T.; Futaba, D. N.; Hata, K.; Fukushima, T. *Adv. Mater.* **2009**, *21*, 1582−1585.

(8) Stoller, M. D.; Park, S.; Zhu, Y.; An, J.; Ruoff, R. S. *Nano Lett.* **2008**, *8*, 3498−3502.

(9) Korenblit, Y.; Rose, M.; Kockrick, E.; Borchardt, L.; Kvit, A.; Kaskel, S.; Yushin, G. *ACS Nano* **2010**, *4*, 1337−1344.

(10) Ma, J.; Tang, J.; Zhang, H.; Shinya, N.; Qin, L.-C. *ACS Nano* **2009**, *3*, 3679−3683.

(11) Portet, C.; Chmiola, J.; Gogotsi, Y.; Park, S.; Lian, K. *Electrochim. Acta* **2008**, *53*, 7675−7680.

(12) Pech, D.; Brunet, M.; Durou, H.; Huang, P.; Mochalin, V.; Gogotsi, Y.; Taberna, P.-L.; Simon, P. *Nat. Nanotechnol.* **2010**, *5*, 651−654.

(13) Bushueva, E. G.; Galkin, P. S.; Okotrub, A. V.; Bulusheva, L. G.; Gavrilov, N. N.; Kuznetsov, V. L.; Moiseekov, S. I. *Phys. Status Solidi B* **2008**, *245*, 2296−2299.

(14) Lin, R.; Taberna, P.-L.; Fantini, S. b.; Presser, V.; Pérez, C. R.; Malbosc, F. o.; Rupesinghe, N. L.; Teo, K. B. K.; Gogotsi, Y.; Simon, P. *J. Phys. Chem. Lett.* **2011**, *2*, 2396−2401.

(15) Portet, C.; Yushin, G.; Gogotsi, Y. *Carbon* **2007**, *45*, 2511−2518.

(16) Zhang, L. L.; Zhou, R.; Zhao, X. S. *J. Mater. Chem.* **2010**, *20*, 5983−5992.

(17) Liu, C.; Yu, Z.; Neff, D.; Zhamu, A.; Jang, B. Z. *Nano Lett.* **2010**, *10*, 4863−4868.

(18) Li, X.; Rong, J.; Wei, B. *ACS Nano* **2010**, *4*, 6039−6049.

(19) Huang, J.; Sumpter, B. G.; Meunier, V.; Yushin, G.; Portet, C.; Gogotsi, Y. *J. Mater. Res.* **2010**, *25*, 1525−1531.

(20) Ohno, H. *Electrochemical Aspects of Ionic Liquids*; Wiley-Interscience: New York, 2005.

(21) Kim, T. Y.; Lee, H. W.; Stoller, M.; Dreyer, D. R.; Bielawski, C. W.; Ruoff, R. S.; Suh, K. S. *ACS Nano* **2010**, *5*, 436−442.

(22) Wang, S.; Li, S.; Cao, Z.; Yan, T. *J. Phys. Chem. C* **2010**, *114*, 990−995.

(23) Feng, G.; Zhang, J. S.; Qiao, R. *J. Phys. Chem. C* **2009**, *113*, 4549−4559.
(24) Feng, G.; Qiao, R.; Huang, J.; Dai, S.; Sumpter, B. G.; Meunier, V. *Phys. Chem. Chem. Phys.* **2011**, *13*, 1152−1161.
(25) Israelachvili, J. N. *Intermolecular and Surface Forces*; Academic Press: New York, 1992.
(26) Vatamanu, J.; Borodin, O.; Smith, G. D. *J. Am. Chem. Soc.* **2010**, *132*, 14825−14833.
(27) Jiang, D.; Meng, D.; Wu, J. *Chem. Phys. Lett.* **2011**, *504*, 153−158.
(28) Wu, J.; Jiang, T.; Jiang, D.; Jin, Z.; Henderson, D. A. *Soft Matter* **2011**, *7*, 11222−11231.
(29) Kornyshev, A. A. *J. Phys. Chem. B* **2007**, *111*, 5545−5557.
(30) Fedorov, M. V.; Kornyshev, A. A. *Electrochim. Acta* **2008**, *53*, 6835−6840.
(31) Fedorov, M. V.; Kornyshev, A. A. *J. Phys. Chem. B* **2008**, *112*, 11868−11872.
(32) Oldham, K. B. *J. Electroanal. Chem.* **2008**, *613*, 131−138.
(33) Lamperski, S.; Outhwaite, C. W.; Bhuiyan, L. B. *J. Phys. Chem. B* **2009**, *113*, 8925−8929.
(34) Georgi, N.; Kornyshev, A. A.; Fedorov, M. V. *J. Electroanal. Chem.* **2010**, *649*, 261−267.
(35) Vatamanu, J.; Borodin, O.; Smith, G. D. *J. Phys. Chem. B* **2011**, *115*, 3073−3084.
(36) Baldelli, S. *Acc. Chem. Res.* **2008**, *41*, 421−431.
(37) Alam, M. T.; Mominul Islam, M.; Okajima, T.; Ohsaka, T. *Electrochem. Commun.* **2007**, *9*, 2370−2374.
(38) Alam, M. T.; Islam, M. M.; Okajima, T.; Ohsaka, T. *J. Phys. Chem. C* **2007**, *111*, 18326−18333.
(39) Lockett, V.; Sedev, R.; Ralston, J.; Horne, M.; Rodopoulos, T. *J. Phys. Chem. C* **2008**, *112*, 7486−7495.
(40) Shim, Y.; Kim, H. J. *ACS Nano* **2010**, *4*, 2345−2355.
(41) Meunier, V.; Kalinin, S. V.; Shin, J.; Baddorf, A. P.; Harrison, R. *J. Phys. Rev. Lett.* **2004**, *93*, 246801.
(42) Borodin, O. *J. Phys. Chem. B* **2009**, *113*, 11463−11478.
(43) Lindahl, E.; Hess, B.; van der Spoel, D. *J. Mol. Model.* **2001**, *7*, 306−317.
(44) Yeh, I. C.; Berkowitz, M. L. *J. Phys. Chem.* **1999**, *111*, 3155−3162.
(45) Hess, B.; Bekker, H.; Berendsen, H. J. C.; Fraaije, J. G. E. M. *J. Comput. Chem.* **1997**, *18*, 1463−1472.
(46) Feng, G.; Huang, J.; Sumpter, B. G.; Meunier, V.; Qiao, R. *Phys. Chem. Chem. Phys.* **2011**, *13*, 14723−14734.
(47) Alam, M. T.; Islam, M. M.; Okajima, T.; Ohsaka, T. *J. Phys. Chem. C* **2008**, *112*, 16600−16608.
(48) Bazant, M. Z.; Storey, B. D.; Kornyshev, A. A. *Phys. Rev. Lett.* **2011**, *106*, 046102.
(49) Vatamanu, J.; Cao, L.; Borodin, O.; Bedrov, D.; Smith, G. D. *J. Phys. Chem. Lett.* **2011**, *2*, 2267−2272.
(50) Chmiola, J.; Yushin, G.; Gogotsi, Y.; Portet, C.; Simon, P.; Taberna, P. L. *Science* **2006**, *313*, 1760−1763.
(51) Ganesh, P.; Kent, P. R. C.; Mochalin, V. *J. Appl. Phys.* **2011**, *110*, 073506−8.
(52) Feng, G.; Cummings, P. T. *J. Phys. Chem. Lett.* **2011**, *2*, 2859−2864.
(53) Jiang, D.; Jin, Z.; Wu, J. *Nano Lett.* **2011**, *11*, 5373−5377.
(54) Wu, P.; Huang, J.; Meunier, V.; Sumpter, B. .G.; Qiao, R. *ACS Nano* **2011**, *5*, 9044−9051.